

# A Statistical Study of Limb Flares Observed by RHESSI: Imaging

Wei Liu, Yanwei Jiang, and Vahé Petrosian

*Department of Physics, Stanford University, Stanford, CA 94305-4060*

liuw@stanford.edu

Thomas Metcalf

*LMSAL, Lockheed Martin Solar and Astrophysics Laboratory, Palo Alto, CA 94304*

## ABSTRACT

Hard X-ray observations by the Reuven Ramaty High Energy Solar Spectroscopic Imager (RHESSI) (Lin, et al. 2002) provide unprecedented opportunities to understand the underlying physics driving solar flares. We have embarked on an investigation of a sample of *limb flares* observed by RHESSI. RHESSI flare images are used to infer flaring loop structures and to distinguish between footpoint, looptop and other possible types of sources. We present an analysis of the lightcurves and images for these features and show statistics on the occurrence of looptop and footpoint sources. These are compared with previous studies utilizing YOHKOH/HXT observations, and their implications for particle acceleration processes and other theoretical aspects of flares are discussed.

## 1. INTRODUCTION

Observations of solar flares are very important tools of studying magnetic reconnection, particle acceleration and other plasma processes, the result of which can have significant implications for other astrophysical phenomena. Observations by low spectral and spatial resolution instruments can give us only the lightcurve and a crude spectrum of the whole flare which may consist of many distinct sources with different characteristics. One of the significant advancement achieved by the YOHKOH satellite is the discovery of distinct looptop (LT) sources in addition to the normal footpoint (FP) sources (Sakao et al. 1994; Masuda et al. 1994). These new observations provide further evidence for stochastic acceleration model (Petrosian et al. 1999, 2002), which was shown to be consistent with the broadband spectra of several solar flares (Park et al. 1997). As suggested by this and other models, these different sources should have different electron distributions and spectra determined by the physical condition at the acceleration site. RHESSI with its unprecedented spectral and spatial resolutions can image at different energy bands. This exceptional imaging spectroscopic capacity, combined with its excellent time resolution, provides us a multi-dimensional pictures of solar flares, which can set stringent constraints on the model parameters and will eventually improve our understanding of the relevant physical processes.

Several bright flares observed by RHESSI have been extensively analyzed in this respect, demonstrating its capabilities. In this paper, we present results from our study of 22 limb flares. We describe the flare selection criteria, the imaging procedure. The advantages and/or weaknesses of different software packages are also discussed. In this paper, we focus on the imaging and lightcurves of the LT and FP sources. The spectra of the sources are presented in a complementary paper (Jiang et al.; poster # 18.03).

## 2. DATA REDUCTION AND ANALYSIS

### 2.1. Sample Selection Criteria

We searched through the online RHESSI flare list (from 12-Feb-2002 through 02-May-2003) for appropriate limb flares, using criteria similar to those introduced by Masuda (1994) and used by Petrosian et al. (2002). These are:

- **Heliocentric longitude**  $\geq 70$  degrees. This provides sufficient angular separation between footpoint and looptop sources. The heliocentric (x, y) coordinates in the RHESSI flare list were converted into heliographic (longitude, latitude) coordinates. For flares whose locations are not available in the list, we obtained the locations by making full disk RHESSI images, usually in the 12-25 keV energy channel about the peak time, and use the position of the brightest pixel as the flare location.
- **Peak count rate**  $\geq 30$  per second per detector in the **12-25 keV channel**, allowing sufficiently good imaging quality.

We then carefully examined the sample flares satisfying these criteria and eliminated those with strong particle events, severe pileup or decimation, poor data quality, etc. 22 flares are included in our final sample. For each event, we performed imaging spectroscopy and lightcurve study as follows.

### 2.2. Imaging

At present, for the purpose of studying spectroscopy and lightcurves of individual sources using RHESSI data, the first step is to reconstruct images in different energy bands and/or time ranges. Key points in our imaging processes are described below.

- **Imaging algorithms.** Among the available RHESSI imaging algorithms, we used 'Back-projection' and 'CLEAN' for preliminary studies, 'CLEAN' for lightcurve purposes as it is relatively much faster, and used much slower 'PIXON' for imaging spectroscopy, which because of its excellent photometry is most suitable for this task.
- **Time Ranges.** Different time ranges were selected for different purposes. For spectroscopic images, a time range about the peak in the 25-50 keV channel

is preferred. For lightcurve images, we selected a time interval including the rising and decaying phase and divided it into a number of time bins (each bin for an image). Each time range (bin) has an appropriate length (a multiple of the spacecraft spin period  $\simeq 4$  seconds) to allow sufficient photon counts for imaging as well as good temporal resolution. All the time ranges (bins) are away from intervals with particle events, with attenuator state changes, or with decimations, with occasional exceptions.

- **Energy Bins.** For imaging spectroscopy, the energy range were set as follows. The lower limit of the energy range was obtained by the attenuator states: namely, about 6 keV when none of the two attenuators is closed, 10 keV when one is in, and 15 keV when both are in. The upper limit goes as high as there are sufficient signals in the images. Once the energy range was obtained we divided it into logarithmically spaced bins with the smallest bin close to the limit of RHESSI's energy resolution, i.e.,  $\simeq 4$  keV. For lightcurves, we took much broader energy bins in each of which images at different energies exhibit common features.

### 2.3. Images and Lightcurves

Once images at different energies or times are obtained, we are ready to infer spectra as well as lightcurves of individual sources. By examining images at various energies and times, we identified footpoint and/or looptop sources. For each source, we selected a box to enclose it and summed over all the pixel values in this box, divided by the width of the energy bin, to get the differential photon flux. If available, Images from Transition Region And Coronal Explorer (TRACE) were used to help distinguish individual sources. Plotting the flux versus energy (time) results in the spectrum (lightcurve) and in turn the characteristics of the spectrum (lightcurve) provides clues on the nature of the source.

Table 1: List of flare events included in this study.

Flare ID (ymmdd#)	Peak time (UT)	Disk position	NOAA AR #	GOES class	Peak Count	Highest E-band (keV)	Notes
2022003	11:06:18	N13W73?	-	C7.5	656	50-100	3 FPs, no LT?
2032819	17:58:18	S04W90	-	C7.6	200	25-50	one source (LP)?
2041509	23:12:26	N21W77	9893?	M1.2	816	25-50	complex <sup>T</sup>
2051706	07:38:10	N13E89?	-	M1.5	1328	25-50	2 LPs?
2051909	21:46:22	S23E78	-	C4.7	84	25-50	source not well def.
2062904	09:29:46	S17E79	-	C2.0	352	12-25	single
2072301	00:30:06	S13E74	0039	X4.8	57379	800-7000	complex <sup>T</sup>
2072307	12:21:42	S19E78	-	C2.9	240	25-50	complex <sup>T</sup> ?
2080327	19:06:54	S16W83	0039	X1.0	28697	25-50	complex <sup>T</sup>
2080602	05:18:18	N17E92	-	C2.1	108	25-50	single?
2081203	02:17:18	S08E86	-	C1.4	160	25-50	single
2082336	16:10:18	S10W88	-	-	104	25-50	single <sup>T</sup>
2082418	11:16:10	S05W89	0069?	-	400	25-50	complex (multi-LPs) <sup>T</sup> ?
2082803	10:59:30	S18W79	0083	C5.7	912	50-100	complex
2082809	18:10:46	N10E87	-	C6.6	784	12-25	one source (LP)
2090309	12:45:42	S08W77	0087?	C1.5	128	25-50	complex
2090608	16:27:02	S06E89	-	C9.2	752	25-50	loop not well def?
2090801	01:39:10	S11E79	0105	M1.5	1072	12-25	complex
2092002	09:26:42	S25E75	0126	M1.8	1520	800-7000	single
2111410	11:09:38	S15E71	0195?	C5.5	352	50-100	2 FPs
2112532	21:50:30	S13W89	-	C?	72	25-50	single
3021411	09:17:18	N12W88	-	M1.2	1072	25-50	one source

Note: (1) Peak counts (counts/s) are in the 12-25 keV energy band. (2) 'single' = single loop; about 6 events are probably of this type. (3) 'complex' = complex morphology; roughly about 8 events fall into this category. (4) 'one source' = only one source was detected; about 3 events have this characteristics. (5) The superscript 'T' denotes those flares with TRACE data available in the RHESSI FOV.

### 3. RESULTS

- **Single Loop Flares.**

Of the 22 total events, 6 appear to be morphologically similar to the canonical Masuda flare, namely, a looptop source connected by a single flaring loop to two footpoints. PIXON images of these flares were obtained around the peak time, and other times whenever the count rate was sufficiently large to allow imaging in the 25-50 keV band. We use these images as the input for imaging spectroscopy (see the accompanying paper by Jiang et al; poster #18.03). We describe **Flare 2092002** which is a GOES M1.8 flare observed by RHESSI up to 800-7000 keV. This event started at 09:22:08UT on September 20, 2002, continued rising to a sub-peak at 09:25:59 in energy channel between 25 keV and 300 keV, and peaked at 09:26:42UT nearly simultaneously in the energy channels from 3 keV through 300 keV as can be seen from the lightcurves in Fig. 1. The HXR images were reconstructed by the PIXON algorithm using front segments of detectors 3 through 6, and detectors 8 and 9, with a minimal spatial resolution of 7". Fig. 2 shows the PIXON images in separate energy bands for a time interval [09:26:36, 09:27:20], covering the main peak. It is clearly shown that in the 11.4-13.4 keV image a diffuse source dominates, suggesting a hot looptop source of  $T \simeq 2.22$  keV. Two footpoint sources appear in about 21.7-25.5 keV and become more and more dominant as the energy goes higher. The boxes in Fig. 1b define the three sources. The corresponding fluxes were calculated from these image with background subtracted (see the Miscellany section). Fig. 3 shows the lightcurves at a cadence of 2 seconds with a  $\simeq 4$  seconds integration time in the 12-25 keV and 25-50 keV band. The ratio of fluxes of the two FPs to the LT source averaged over the rising, peak, and decaying phase, respectively, is shown in red. Again, we note that the looptop source dominates in 12-25 keV and its importance gradually increases with time; in contrast, the footpoint sources are much brighter in the 25-50 keV channel but it decays more rapidly after the peak. Flares 2081203 and 2112532 have qualitatively similar characteristics (see Fig. 4 through 9).

- **Multiple Loop Flare.**

Many flares appear to have a more complex morphology similar to the flares studied by Petrosian et al. (2002) during the rising phase of this sunspot cycle. An example of such a case is **Flare 2080327** (see Fig. 10 through 12).

- **Miscellany.** In few cases not both looptop and footpoint are present. Based on their locations, lightcurves and spectra, some of these appear to be a loop-

top source; e.g. [Flare 2082809](#)(Fig. 13) and some footpoint sources; e.g. [Flare 2111410](#). (Fig. 14 & 15)

#### 4. SUMMARY & DISCUSSIONS

**Miscellaneous statistics** We have analyzed a sample of 22 limb flares observed by RHESSI, 10 of which have lightcurves of individual LT and FP sources obtained (See Fig. 16 for the distribution of flare locations). Out of this sample, about 6 flares exhibit a classic single loop structure (i.e., with one looptop and two footpoint sources); about 8 have complex morphology; 3 flares appear as a single looptop source. Among the complex flares, we identified one as a multiple-loop events similar to those found by Petrosian et al. (2002); for other complex events further analysis of lightcurves and imaging spectroscopy, as well as multiple-wavelength observation is needed to distinguish individual sources.

#### **Statistics of the relative fluxes: footpoints v.s. looptops.**

- The footpoint to looptop flux ratios reveal that looptop sources are much softer in spectrum than footpoint sources (see the lower right panel in Fig. 17). At lower energies (e.g.,  $\leq 25$  keV), the median of FPs/LT flux ratios is very close to 1 ; in contrast, for higher energies (e.g.,  $\geq 25$  keV), the median ratio is much greater than unity and its distribution is much flatter. These results are consistent with theoretical calculations (see Liu and Petrosian, poster #16.05).
- At flare peaks, the looptop emission dominates in low energies and footpoints dominate in high energies (Fig 17, lower left panel).
- In the decay phase of a flare (see upper panels of Fig. 17), the looptop source tends to be the major contribution to the total flare emission, especially in low energies (e.g.,  $\leq 25$  keV).

## Miscellany

- **Detector selection.** For spectroscopic 'PIXON' images, the front segments of detectors 3, 4, 5, 6, 8, and 9 were used by default (with a few exceptions). Detector 2 was deselected for its threshold at about 25 keV and poor energy resolution of about 9 keV. Detector 7 was not included either because of its resolution of about 3 keV. We did not use detector 1 because its 2" spatial resolution is smaller than most of the smallest features in our sample. For lightcurve 'CLEAN' images, usually detector 3 through 8 were used.
- **Background estimate.** Since RHESSI is non-shielded spacecraft, the background in the data is high (Smith, 2002). There is no well-defined algorithm to subtract background for imaging at present. To roughly estimate the DC background in images, we simply selected a sufficiently large box to enclose all the major flaring sources. Next we took the averaged pixel value in the image excluding the selected box as the background contribution to each pixel. For a boxed source with  $N$  pixels, the background in the flux can be estimated as

$$b = \frac{N}{w} \times \frac{1}{M} \sum_{i=1}^M p_i,$$

where  $p_i$  is the individual pixel values (photons  $\text{cm}^{-2} \text{s}^{-1} \text{arcsec}^{-2}$ ) in the image outside the selected box,  $M$  is the number of pixels there, and  $w$  is the width of the energy bin.

- **Error estimate.** The error estimate for RHESSI images is still a research program. Our first attempt was to use the 'hsi\_calc\_image\_error.pro' routine in the Solar Software (SSW) IDL package to get the pixel by pixel error,  $\sigma_i$ , in an image. These errors are intended to give a measure of how well constrained each pixel is by the data given the image model derived from the reconstruction. The IDL routine determines how large a change in the image is required to make a one sigma change in the fit. The error for a source flux with  $N$  pixels and energy bin width  $w$  is

$$\sigma = \frac{1}{w} \sqrt{\sum_{i=1}^N \sigma_i^2}.$$

**Acknowledgments** The work at Stanford is supported by NASA grants NAG5-12111, NAG5 11918-1. T. Metcalf would like to acknowledge support from grant NAS-98033-05/03. The authors would like to thank Dr. Kim Tolbert and Dr. Säm Krucker for their kind help with RHESSI software and data analysis.

## REFERENCES

- Lin, R., et al., 2002, Solar Phys., 210, 3  
 Masuda, 1994, Ph.D. Thesis, Univ. Tokyo  
 Petrosian, V., Donaghy, T. Q., and McTiernan, J. M., 2002, ApJ, 569, 459  
 Smith, D. M., et al., 2002, Solar Phys., 210, 33  
 Jiang, Y., et al., this poster session, SPD 2003  
 Liu, S. and Petrosian, V., SPD, 2003

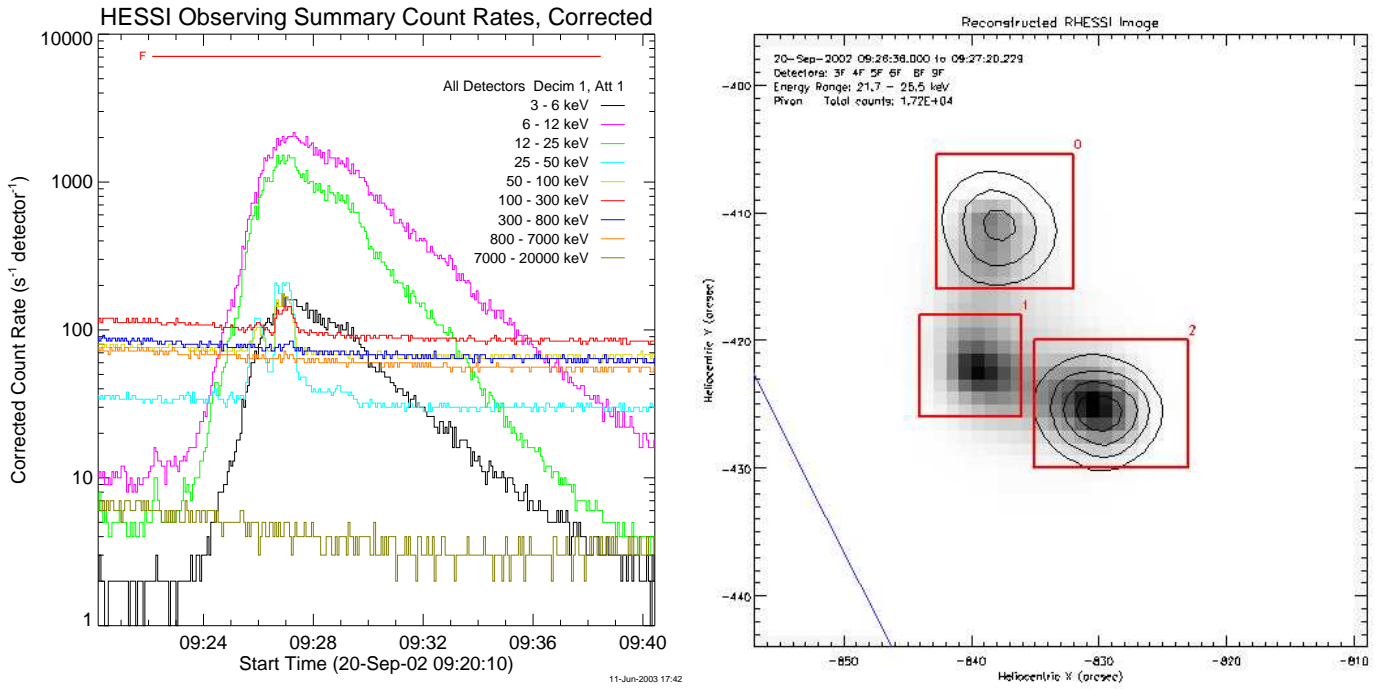


Fig. 1.— The 2092002 flare: lightcurves (left) and hard X-ray images with boxes defined to enclose individual sources (right).

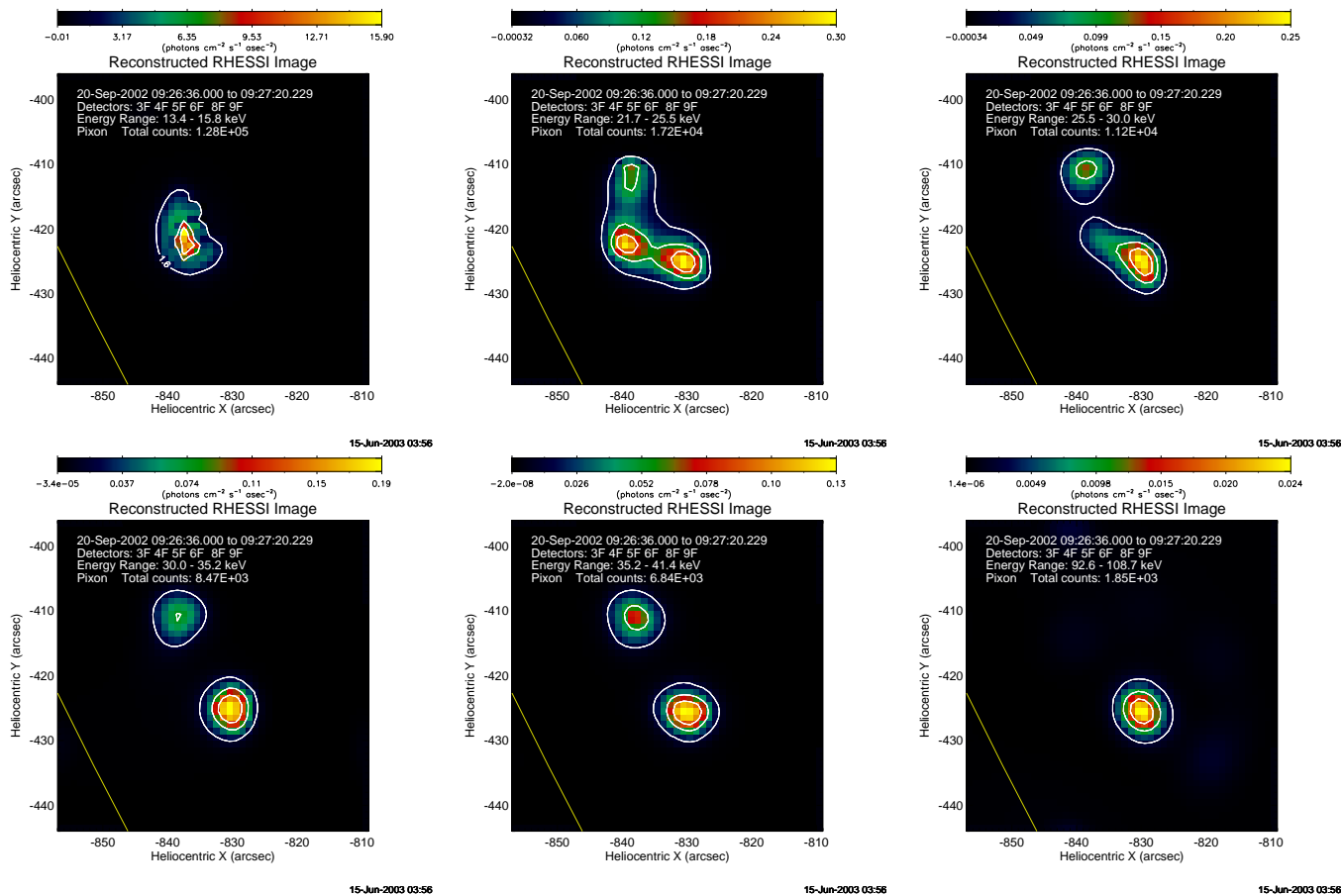


Fig. 2.— Hard X-ray images of the 2092002 flare at different energies. The contour levels are at 10, 40, 70% of the maximum of each panel. The solar limb is marked in yellow. Note the south footpoint is much brighter than the north one, which may be due to possible asymmetric convergence of the flaring loop. That is, the loop may converge much rapidly approaching to the north FP and this result in stronger mirroring effect which suppresses high energy electrons from bombarding the chromosphere there. Electrons can escape the loop much readily from the other end of the loop (the south FP), producing a stronger thick target source there.

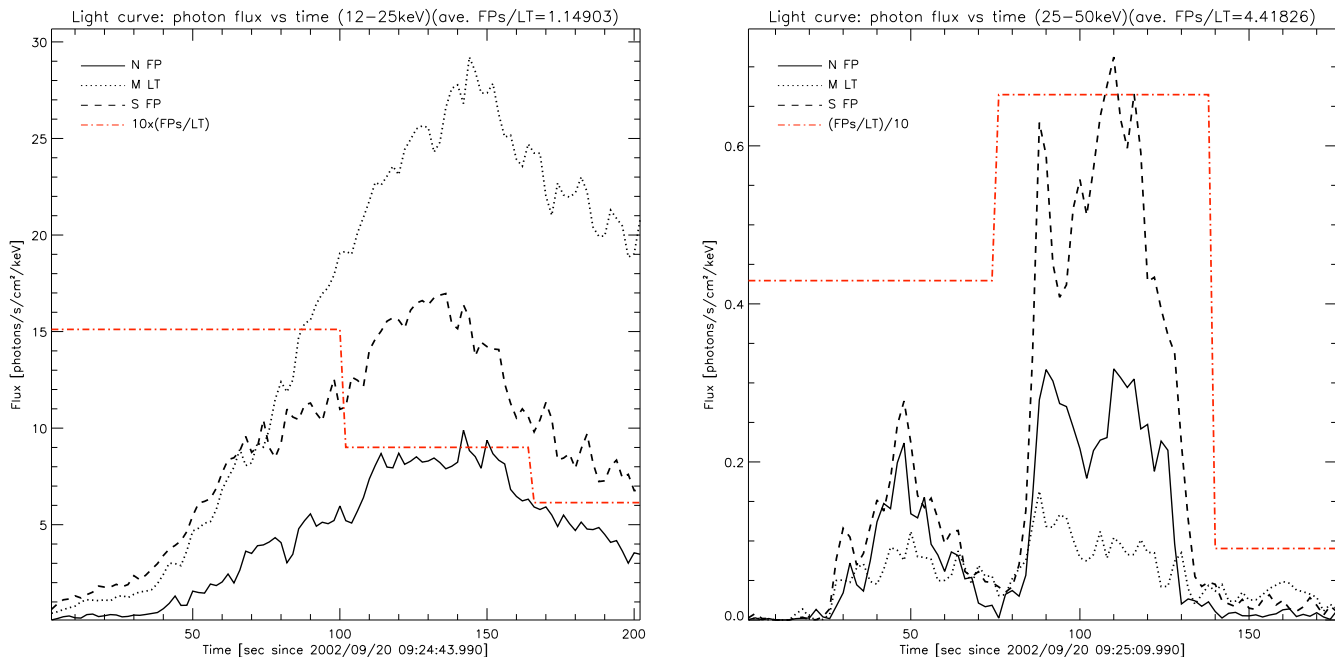


Fig. 3.— Light curves of individual footpoint and loop-top sources in the 12-25 keV (left panel) and 25-50 keV (right) energy band for the 2092002 flare. The dot-dashed, step-shaped curves show the ratio of flux of the two FPs to the LT sources, averaged over time intervals before, during, and after the peak. 'N FP' refers to the northern looptop, 'M FP' the middle footpoint, 'S LP' the southern footpoint. We note there are two distinct pulses in the 25-50 keV band. From the first pulse to the second, the LT emission is essentially constant in the 25-50 keV band but increases substantially in 12-25 keV. This suggests the LP spectrum undergoes softening, which may be explained by the evaporated chromospheric material dominating the LP emission.

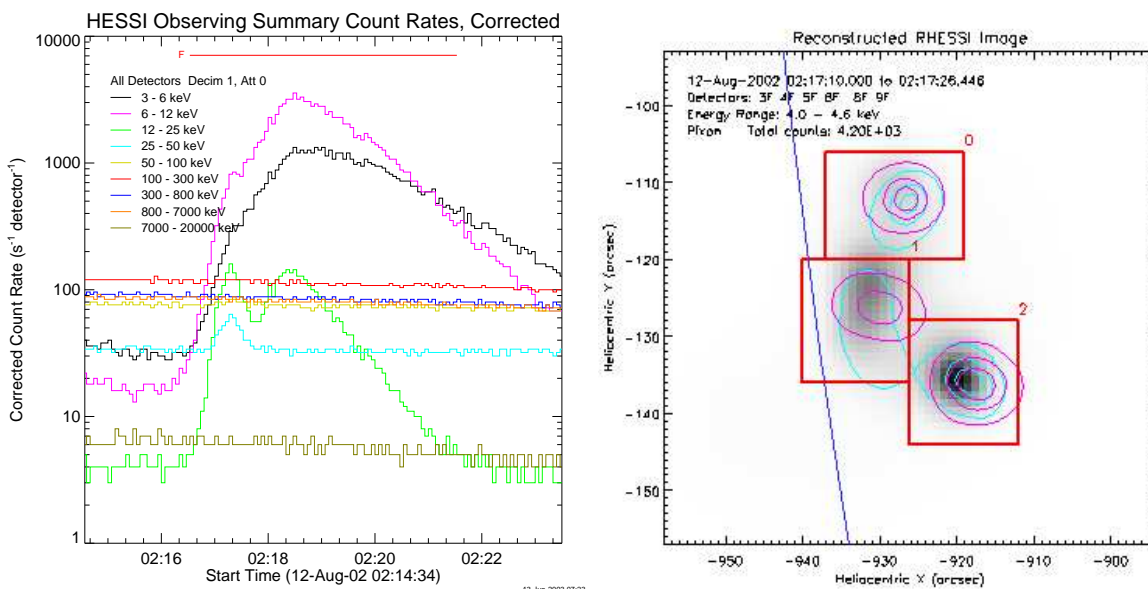


Fig. 4.— Light curves (left) and source box definition (right) of the 2081203 flare.

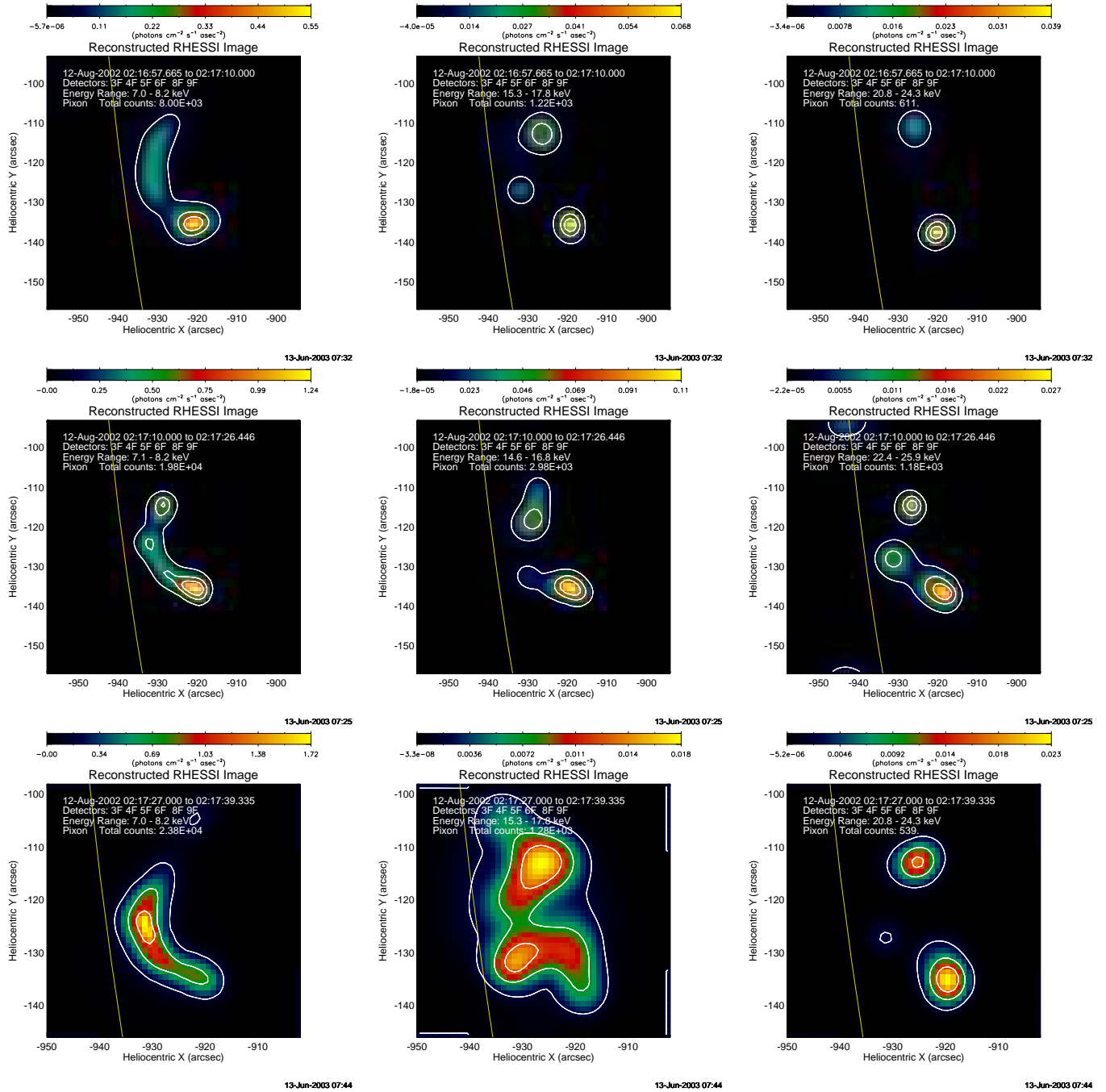


Fig. 5.— PIXON images of the 2081203 flare at separate energies and times. The upper, middle and lower row corresponds to the rising, peak and decaying phase about the peak time, respectively. Energy goes higher from left to right columns. The temporal evolution indicates that: (i) in lower energy bands, the compact footpoints are the brightest sources in the rising and peak phase, but in the decay phase the looptop dominates and the emission tend to spread over the whole loop; (ii) in higher energy channels, the looptop ephemerally shines at the peak and rapidly dies away but the footpoints remain longer after the peak.

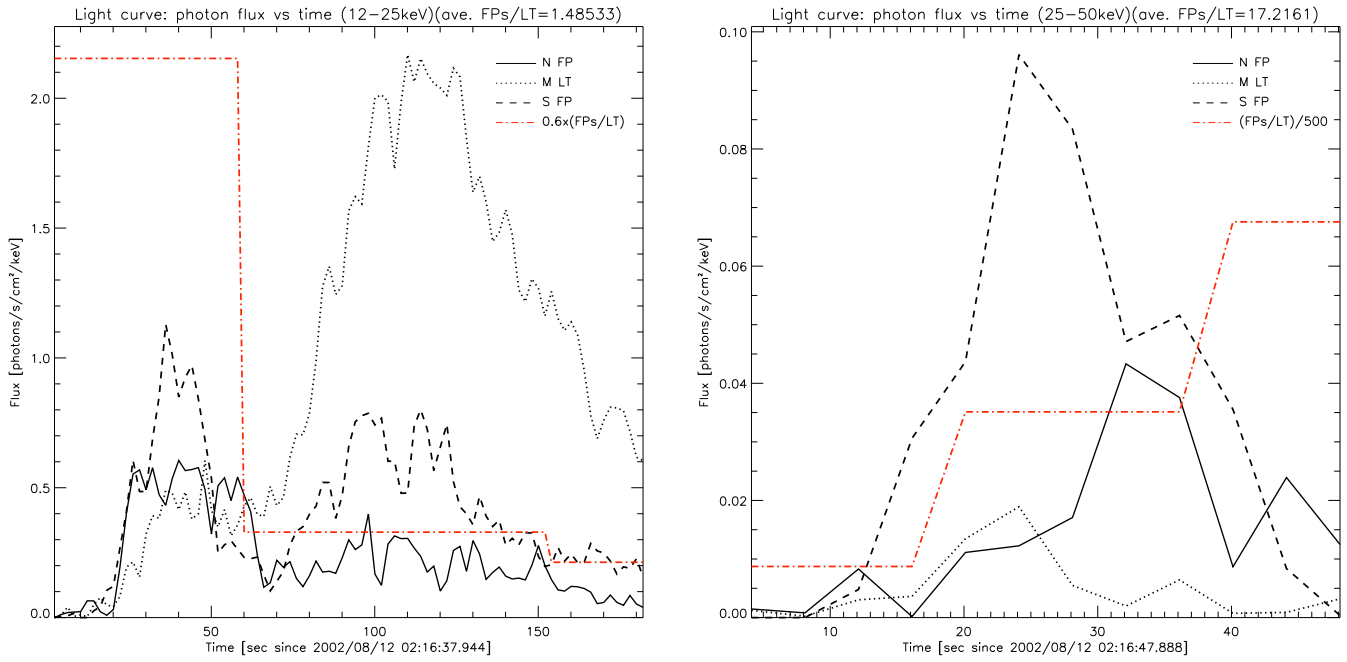


Fig. 6.— Same as Fig. 3 for the 2081203 flare.

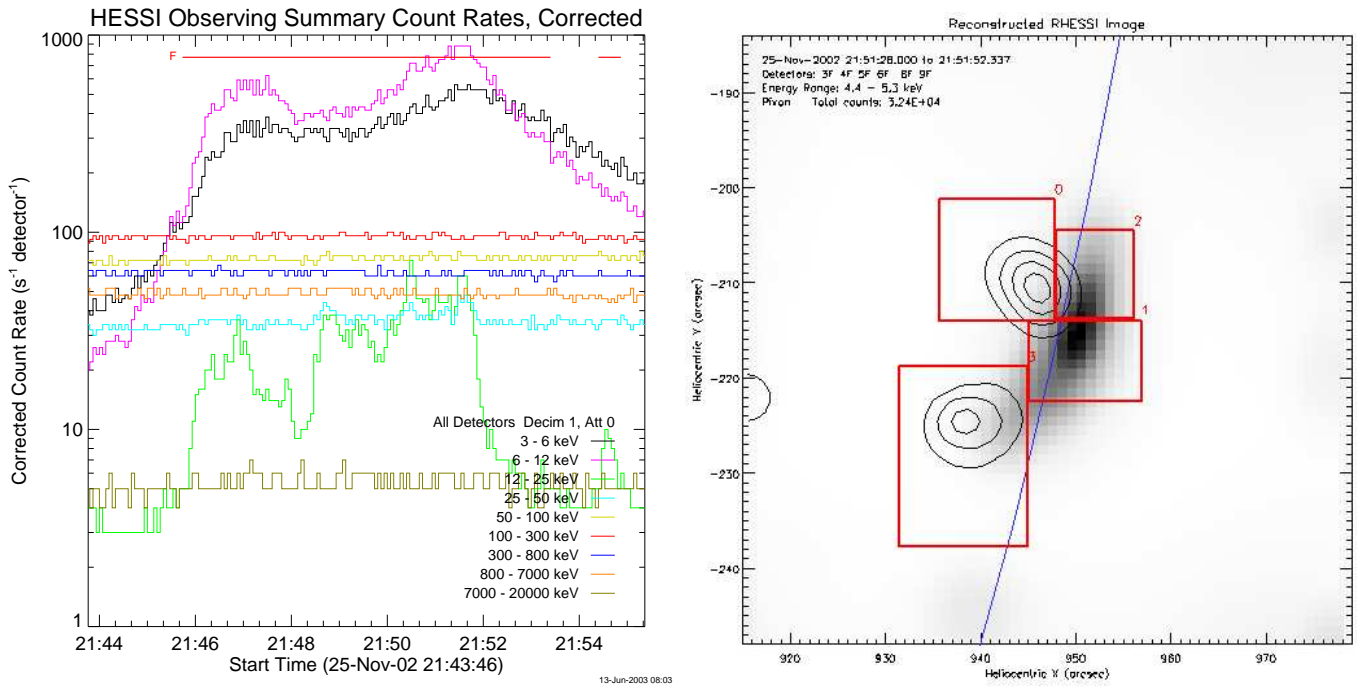


Fig. 7.— Light curves (left) and source box definition (right) of the 2112532 flare.

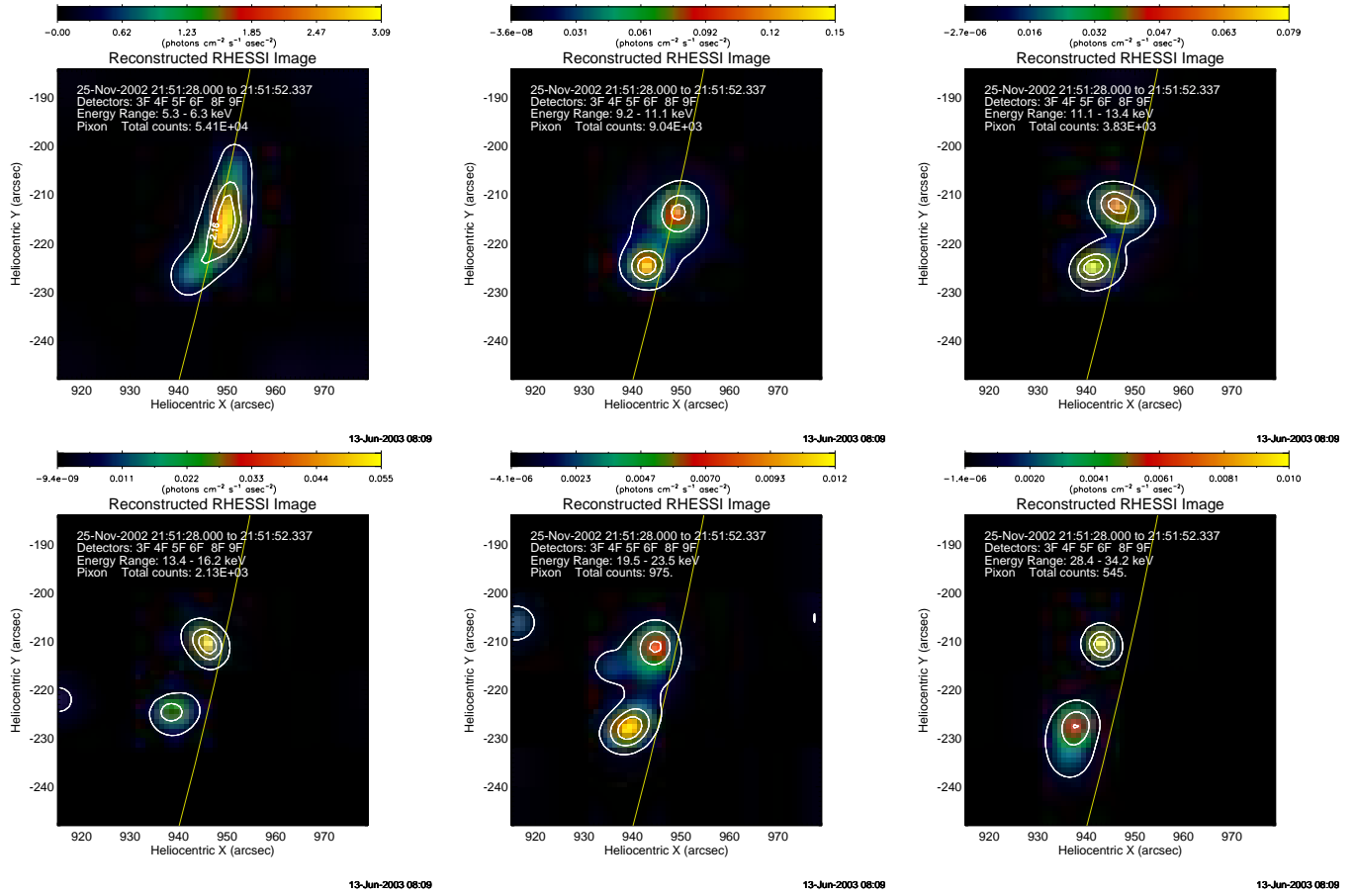


Fig. 8.— RHESSI HXR images of the 2112532 flare.

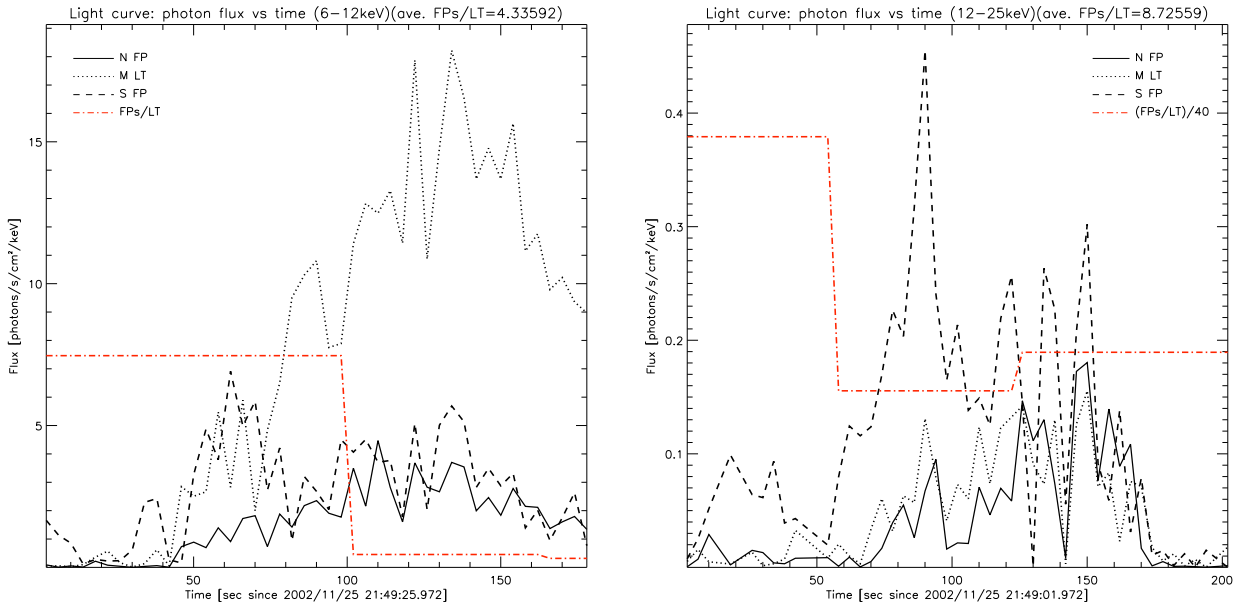


Fig. 9.— Light curves of individual footpoint and loop-top sources for the 2112532 flare (same format as Fig. 3).

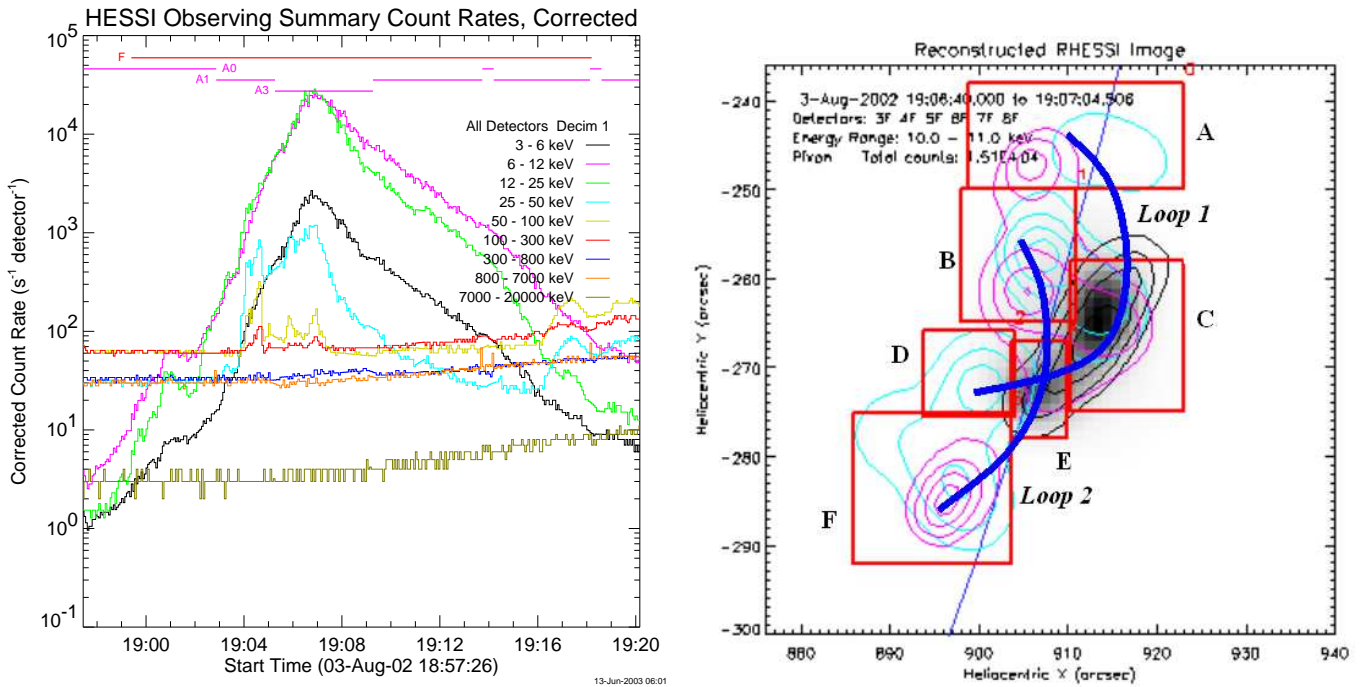


Fig. 10.— Lightcurves of the 2080327 flare (left) and the source box definition (right). Contours and map are PIXON images at different energies. Two major flaring loops are identified, marked in thick, blue lines, and their corresponding looptop and footpoint sources are assigned a letter, A, B, C, etc.

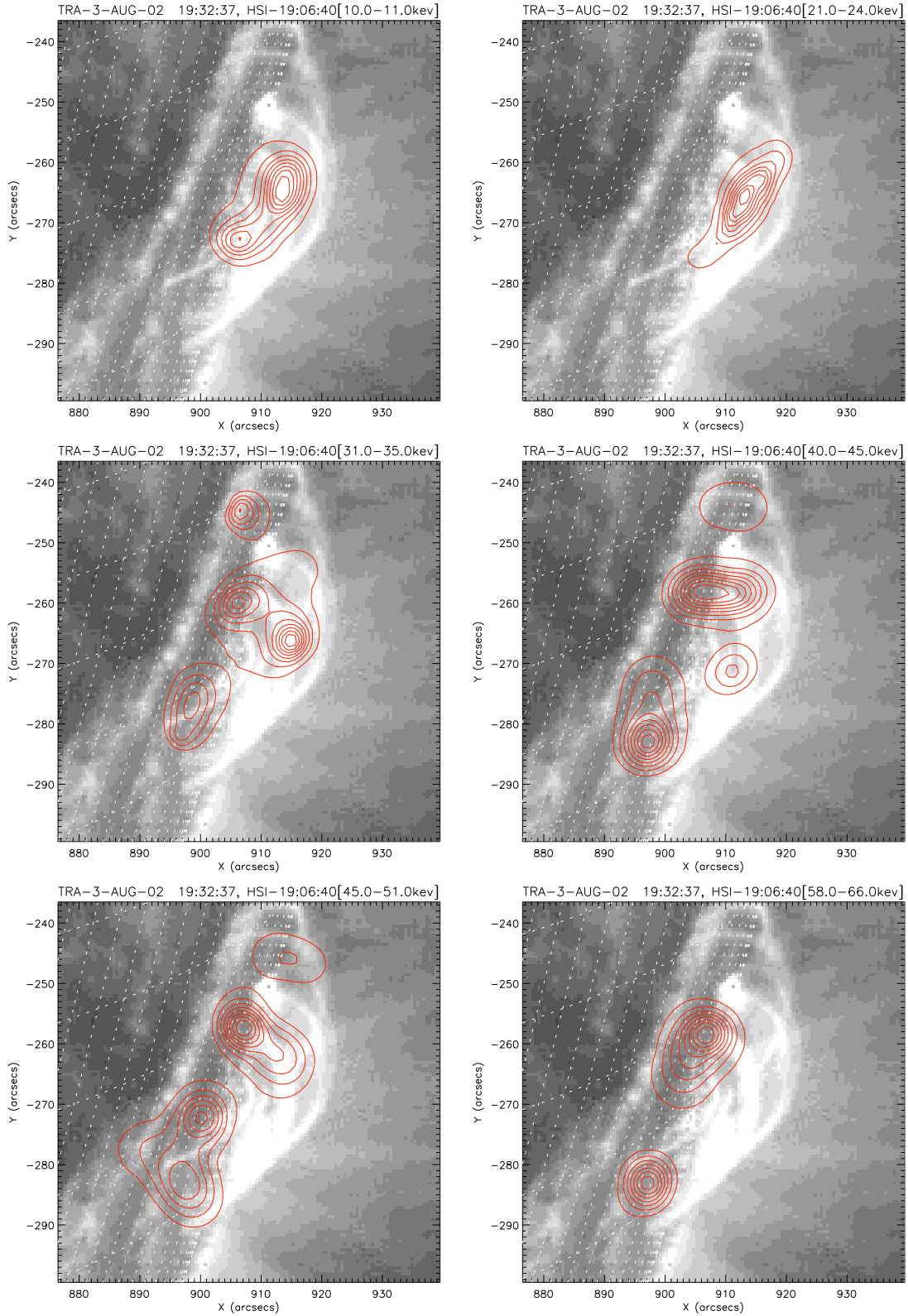


Fig. 11.— RHESSI HXR contours (by PIXON) at different energies overplotted on TRACE 171 Å images for the 2080327 flare. Heliographic grids (dashed lines) have a  $1^\circ$  spacing in both longitude and latitude. Note the TRACE images are at a later time which is best for one to see coronal loop structures in EUV. The TRACE images indicate that there are a series of magnetic loops and two of them are co-located with the RHESSI flaring sources (also see Fig. 10).

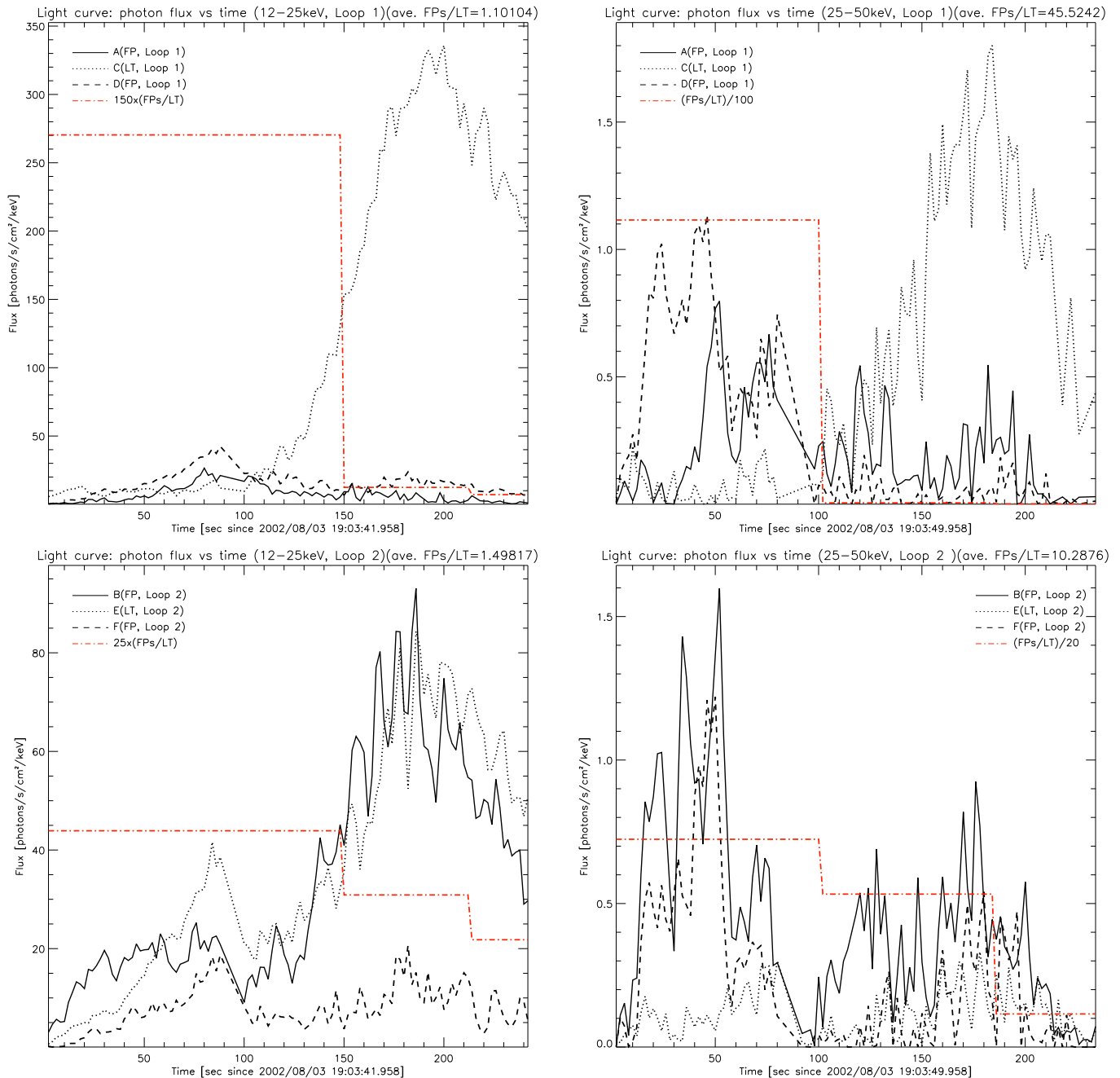


Fig. 12.— Light curves of individual footpoint and looptop sources for the 2080327 flare (same format as Fig. 3). The upper panels are for loop 1 (refer to Fig. 10) in 12-25 keV (left) and 25-50 keV (right); the lower panels are for loop 2. It is interesting to note that the two loops do not contribute equally to the total emission: (i) in the 25-50 keV band, the total flux of loop 2 is higher in the first pulse but lower in the second than that of loop 1; (ii) in the 12-25 keV channel, the looptop of loop 2 is stronger than that of loop 1 by a factor of about 2 in the first pulse (although their total fluxes are comparable at this time) but much weaker by a factor of 4 in the second (loop 2’s total flux is lower too). The looptop emission from loop 1 predominates over others in the second (major) peak in both energy channels. In the 25-50 keV band, the total flux of loop 1 (2) increases (decrease) from the first peak to the second. This suggests that the burst of loop 1 may be initiated by its interaction with loop 2. Please refer to the accompanying poster (# 18.03) by Jiang et al. for the spectroscopic characteristics of the individual sources.

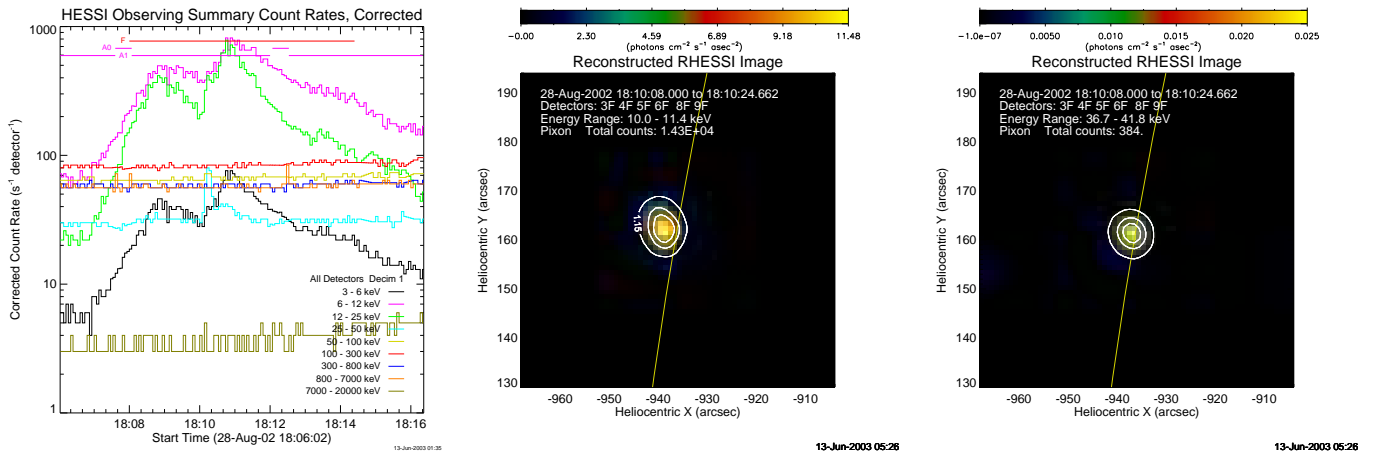


Fig. 13.— Light curves (left) and images (others) at different energies of the 2082809 flare. In our PIXON images about the peak time, this flare appears as a single source on the limb in all the 13 energy bins from 10 to 54.2 keV. CLEAN images at different times also indicate a single source. The full spectrum yields a fit with a power law index of 5.0 and temperature 1.9 keV, suggesting this source is a looptop, presumably with its corresponding footpoints naturally occulted behind the limb.

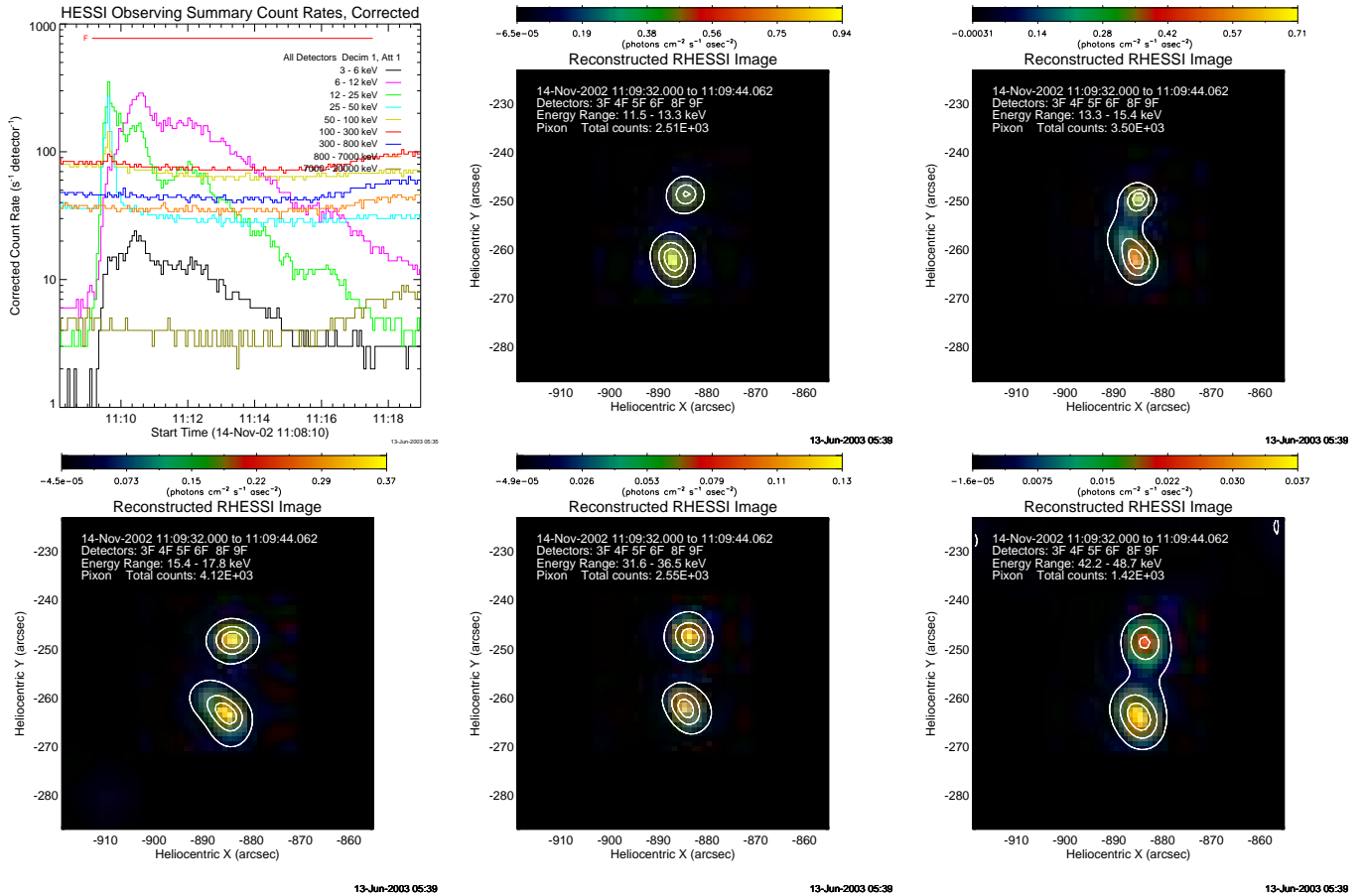


Fig. 14.— Light curves (upper left panel) and images (others) at different energies of the 2111410 flare. From images, this flare does not show an appreciable looptop source possibly because the looptop is too faint to be detected (i.e., out the dynamic range) and/or the angular separation is not sufficient between the LP and FPs, considering its low heliocentric longitude of  $71^\circ$ , the lowest in this sample of the 22 flares.

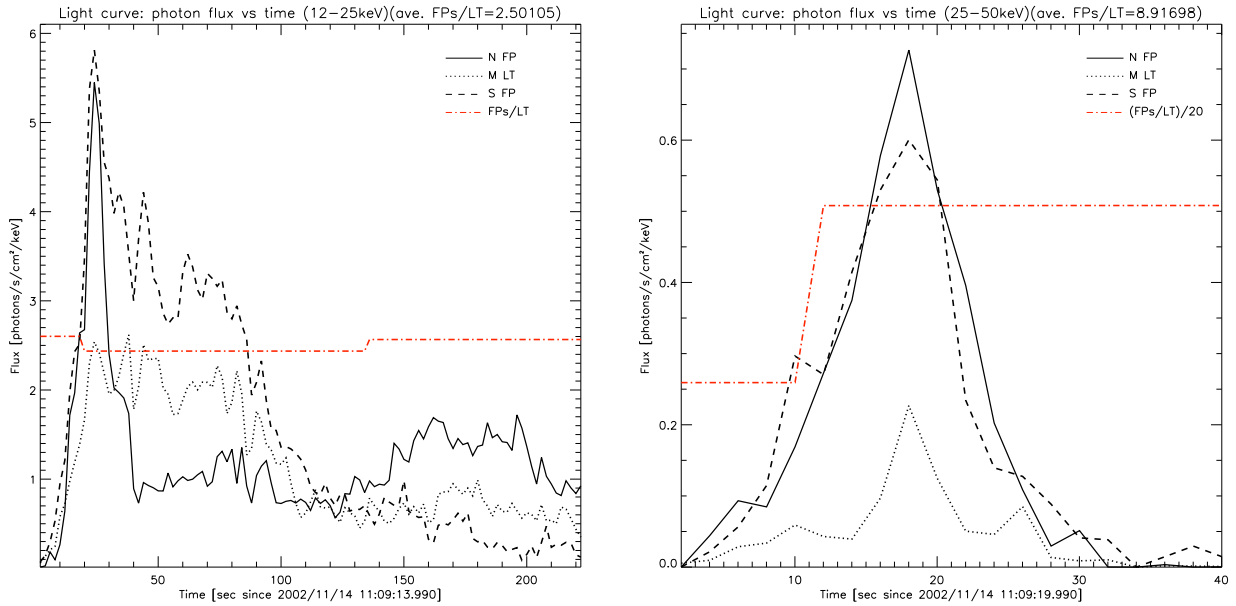


Fig. 15.— Light curves of individual footpoint and loop-top sources for the 2111410 flare (same format as Fig. 3).

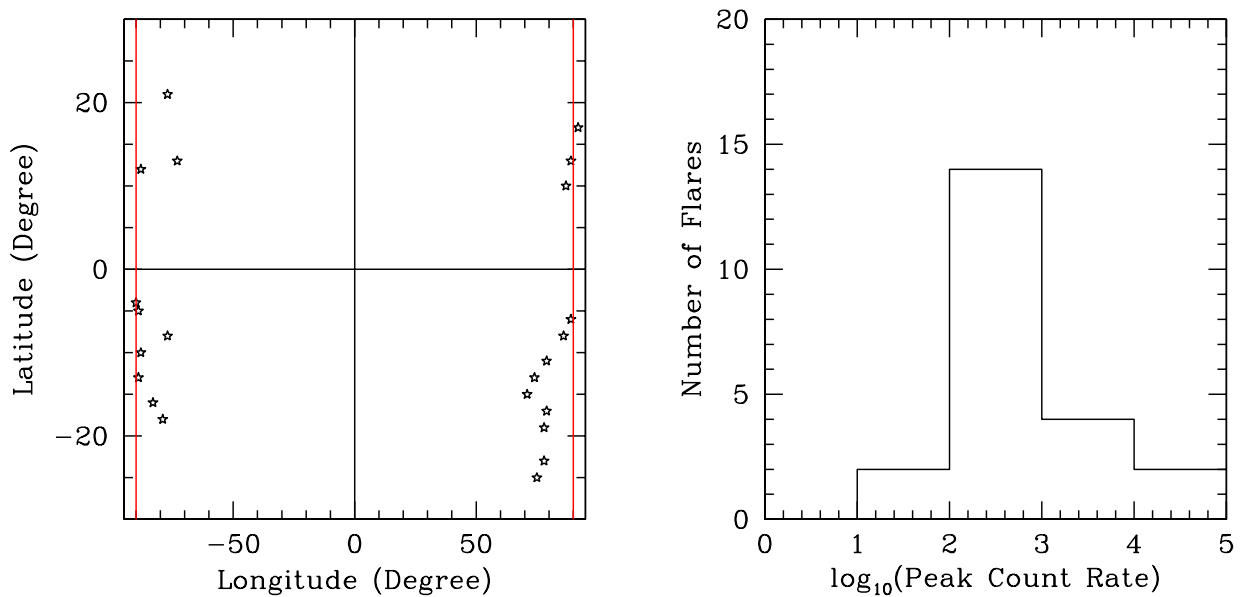


Fig. 16.— The heliographic location distribution (left) and the histogram of the peak count rate (right) of the sample flares. The red vertical lines in the left panel marks  $90^\circ$  in longitude (see Table 1).

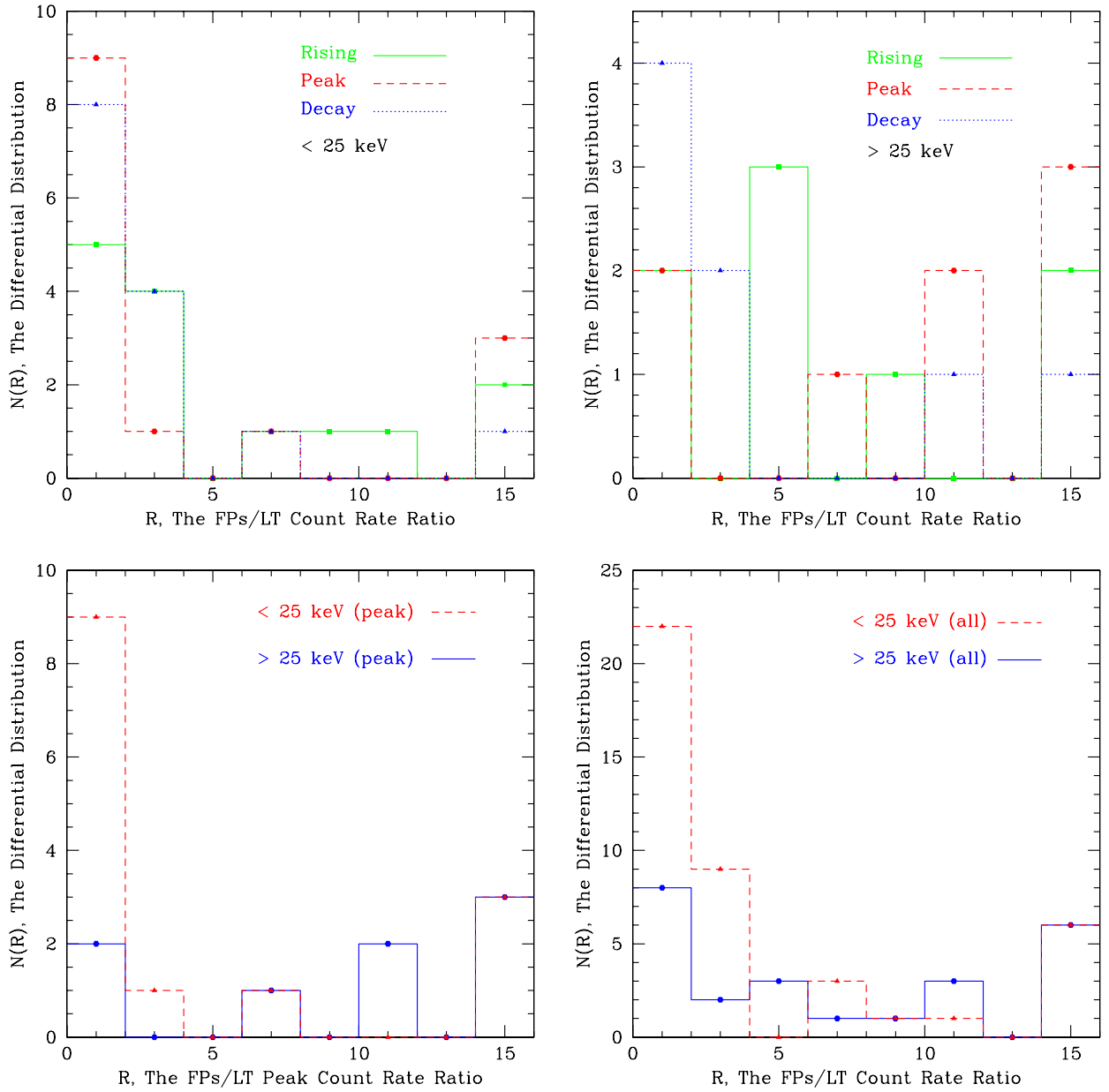


Fig. 17.— Histograms of  $R$ , the FPs to LP flux ratios at different times and energies, with a bin size of 2. The upper cutoff is set at 16, about the upper limit of RHESSI images, and any ratio greater than this value is counted to the last bin (note this results in the tail bump at  $R = 16$ ).